ELSEVIER

Physica A 297 (2001) 495–508

PHYSICA A

www.elsevier.com/locate/physa

# Bursts and cavity formation in *Hydra* cells aggregates: experiments and simulations

José C.M. Mombach[a,*], R.M.C. de Almeida[b], G.L. Thomas[b], A. Upadhyaya[c], J.A. Glazier[c]

[a] *Centro de Ciências Exatas e Tecnológicas, Universidade do Vale do Rio dos Sinos, 93022-000 São Leopoldo, RS, Brazil*

[b] *Instituto de Física, Universidade Federal do Rio Grande do Sul, Caixa Postal 15051, 91501-970 Porto Alegre, RS, Brazil*

[c] *Department of Physics, University of Notre Dame, Notre Dame, IN 46556, USA*

Received 23 March 2001

**Abstract**

We present experimental results and a simulation in two dimensions of the expansion and bursting of aggregates of *Hydra* cells formed from an initially disordered mixture. In the experiments, after cell sorting, the aggregate rounds and swells until violent bursts occur, forcibly expelling internal fluid and loose cells. We use Monte Carlo techniques to simulate the bursts in two dimensions. Initially, we consider a ring made of a monolayer of cells enveloping an internal fluid. Each cell and the internal medium have their areas controlled by target area size. Increasing the target area of the internal cavity causes the aggregate to swell. We observe that aggregates of cells with higher surface tension generate higher internal pressure. In the simulations the cell ring bursts when it is too thin to endure fluctuations in the cellular membranes. The process is relevant to embryonic development. 

*PACS:* 87.10.+e; 87.19.Rr; 68.10.Cr; 75.10.Hk

*Keywords:* Hydra regeneration; Cell sorting; Differential adhesion model; Development

## 1. Introduction

Morphogenesis presents many questions related to how tissues self-organize during embryonic development. The DNA of living organisms stores the required information

* Corresponding author. Fax: +55-51-590-8162.

*E-mail addresses:* mombach@exatas.unisinos.br, jose@if.ufrgs.br (J.C.M. Mombach).


PII: S0378-4371(01)00199-6

more as a recipe than as a body plan, in the sense that many morphogenetic processes take place with their time evolution strongly determined by inescapable physical and chemical laws. The understanding of the dynamics of these phenomena is made difficult by the diversity of parameters and mechanisms acting simultaneously and, most of the time, non-linearly. Strictly controlled experiments and environments provide high valued opportunities to constrain some of these variables.

Cavity formation is important in morphogenesis. It appears very early in phylogenetic evolution and is present in almost all multicellular organisms. For example, blastulation is the stage of the developing animal embryo that results from the cleavage of a fertilized egg. This stage resembles a hollow ball with the dividing cells of the embryo forming a layer around a central cavity [1]. What triggers cavity formation and what mechanisms participate in its development are issues under investigation.

Several simple organisms like *Hydra* and marine sponges can regenerate a functional organism from a compact random cell aggregate obtained by centrifuging dissociated cells [2]. *Hydra* is a simple animal whose cylindrical body is formed by two cell layers (inner endoderm and outer ectoderm) separated by an extracellular matrix (mesoglea) and enveloping the gastric cavity. This simple body plan makes *Hydra* especially useful as a model of cavity formation, since during regeneration endodermal and ectodermal cells must sort, produce mesoglea, and rebuild the gastric cavity.

Regeneration begins with the aggregates rounding up until they become spherical, with cell types sorting to form two concentric layers [3]. In some sense, the sorting process resembles the phase segregation of mixtures of non-miscible liquids, e.g., a small amount of oil mixed with water. The water and oil segregate, with the oil forming discs on the water surface. These disks then coalesce. More generally, two liquids codispersed in a container may either mix or phase separate, depending on the interfacial tension between them. Steinberg [4] first suggested the analogy between dissociated cell mixtures and codispersed liquids, proposing a biological analogue to the surface tension. In analogy to liquids, the aggregates may reach configurations that are energetically stable due to the ability of cells to move under the competitive influence of adhesion forces and membrane fluctuations driven by the cytoskeleton, that here play the role of thermal noise and allow the cells to diffuse through the aggregate. Adhesion forces between biological cells are due to specialized adhesion molecules expressed on the cell surface. Different cell types selectively express different members of the many families of adhesion molecules, resulting in different adhesion intensities between cell types. Experiments have confirmed that aggregates of biological cells present features that are analogous to highly viscous liquid behavior, including surface tension [4,5]. The differential adhesion theory then proposes that forces generated by surface tension play an important role in the position rearrangement of cells in aggregates e.g., the sorting of ectodermal and endodermal cells in *Hydra* [6–8].

For *Hydra* cell aggregates to regenerate into fully functional organisms, the aggregate must establish the correct ratio between the numbers of endodermal and ectodermal cells. Recent numerical studies predict that relative concentrations of different cell types may affect the dynamics of cell sorting [9,10]. Aggregates with initial ratios far from

1 : 1 by volume tend to slough off the excess cell type into the surrounding medium [11], suggesting that the ectodermal cells at the endodermal–ectodermal bilayer interface become polar, reducing their apical adhesivity to cause the excess cells to detach. We are currently investigating this regulation mechanism in more detail, but in the simulations we present in this paper we assume isotropic cells since our model considers only a monolayer of cells with no mesoglea, which is correlated with the polarity of the cells.

In this paper we experimentally investigate the initial stages of *Hydra* cell aggregate regeneration after cell sorting, namely, cavity expansion and ectodermal and endodermal monolayer formation, which relate to the physical and chemical processes underlying gastric cavity formation. This artificial experiment reduces the significance of regulatory gene programs since all cells are adult and differentiated and no differentiation from endoderm to ectoderm occurs [12]. We also numerically simulated differential adhesion mechanisms using a two-dimensional extended Potts model. In the simulations, differential adhesion and osmotic pumping suffice to explain gastric cavity formation in *Hydra*, qualitatively reproducing its main events.

## 2. Material and methods

In our experiments, we dissociate several animals into single cells using standard protocols [13]. We breed normal *Hydra vulgaris* in a disease-free culture at 18°C. We then choose 20–30 starved animals and cut off their heads and feet. We wash them 3 times with ice-cold *Hydra* medium (HM) and twice with ice-cold dissociation medium (DM). We incubate in the DM for about 30 min, place the bodies on a glass plate and chop very finely with a single edged razor blade. We then break the tissue into cells and cell clusters by vigorous pipetting in a test-tube. Filtering the cell solution through a 53 μm mesh produces a suspension with only single cells and small cell clusters. We centrifuge the cell suspension at 1500 rpm for 7 min to form a firm pellet consisting of a random mixture of the two *Hydra vulgaris* cell types. We remove the pellet and cut it into small aggregates, 200–400 μm in diameter. We place each aggregate in a cell well for observation with an inverted optical microscope (Olympus IMT-2). The microscope feeds a CCD camera connected to an S-VHS video recorder and a computer. We monitor the different stages of aggregate development by capturing images and digitizing at regular time intervals. In some cases, we make time lapse movies to view cell movement during reorganization.

## 3. Experimental results

Twelve hours after centrifugation, the pellet rounds up, forming a spherical aggregate with a layer of less cohesive ectodermal cells surrounding an endodermal cell layer and a core of partially sorted cells. After rounding, the aggregate swells, almost

doubling in size 15–16 h after centrifugation. After 17–20 h the endo-ectoderm bilayer separates from the rest of the cells in the interior which now loosely float in the liquid accumulated in the internal cavity.

The swelling appears analogous to the building up of an internal liquid pressure slightly larger than the external medium pressure [14] which in an intact animal prevents the gastric cavity from collapsing. Possible mechanisms include: (i) passive osmotic equilibration through cell membranes, since the external medium is hypotonic to the interior of the aggregate, e.g., if the internal cells lyse due to lack of oxygen or due to lack of diffusion of excreted potassium, (ii) active ionic pumping, which is known to function in intact bilayers from adults, and (iii) diffusion through extracellular channels. Besides swelling, the aggregate starts reorganizing: the outer layer of ectodermal cells and underlying layer of endodermal cells are epithelial in nature and probably become polarized due to the appearance of mesoglea between them. In the regenerating aggregate, qualitative changes in the contact surfaces between individual cells probably stabilize the cavity: the formation of mesoglea between the layers and of gap junctions and other junctions within the endodermal and ectodermal monolayers prevent leakage of liquid from the cavity into the external medium. Previous studies have shown that, for large aggregates that form many heads after full regeneration, no immunofluorescent signal for mesoglea appeared until about 17 h after pellet formation [15,16], consistent with our observation that about this time the excess internal cells separate from the ecto-endoderm bilayer and float loosely in the increased internal cavity liquid. This means that the cells have already become polarized. Furthermore, as our aggregates were small, forming only one head after full regeneration, cell sorting times are shorter and we expect earlier mesoglea formation and polarization.

In an intact animal water expulsion through the mouth periodically compensates for the constant liquid influx. In the regenerating aggregate before body reorganization, this expulsion is not possible since a mouth has not yet formed, so the aggregate swells. At some critical size, a hole opens up in the visibly thin cell layers and the aggregate bursts, forcibly expelling the contents of the interior, including fluid and loose cells. Bursting repeats a few times before the aggregate starts elongating to regenerate a new animal. Typically, the first burst happens after 21 h of pellet formation, but this time may vary with aggregate initial size. Fig. 1 shows a few stages of the cavity formation in *Hydra* cell aggregates.

## 4. Simulations

We consider here numerical simulations of cavity expansion and bursting in two-dimensional cell aggregates. The model [17–21] is based on the differential adhesion hypothesis and is defined as follows: at each site $(i, j)$ of a square lattice with dimensions $L \times L$ we define a spin that may assume any integer value (a Potts spin). The set of all sites with equal spin $S$ defines a cell, labeled by $S$. We consider

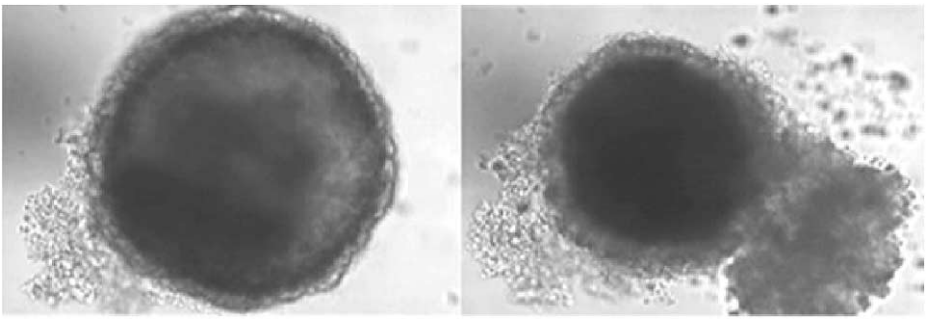

Fig. 1. Microscope images of an experimental aggregate before and after bursting. The aggregate has approximately $10^5$ cells and is 400 μm in diameter.

three major mechanisms acting simultaneously: adhesion between cells, internal pressure that prevents the cells from collapsing, and random fluctuations of cell membranes.

Adhesion between cells originates in the interaction between each spin and its 20 surrounding neighbors (up to fourth neighbors to avoid pinning to the square lattice). The lowest interaction energy, here taken as zero, happens between equal spins, simulating the absence of surface tension between sites belonging to the same cell. The energy between different cells is taken to be positive and when different types of cells are considered, the interaction energy may also be different, depending on the types involved in the interaction. Actually, the intensity of each possible interaction must be specified. Hence, for example, for a system made of an aggregate of cells of one type only plus internal liquid and external medium we must define the values for the interaction between spins belonging to different cells, to a cell and internal medium, to a cell and external medium, and finally between external and internal media. This results in a surface energy term that describes the interaction between contacting cells and between cell and media. It is proportional to the shared interface length, with a proportionality constant depending on the neighboring cell types to reflect differential adhesion strengths (from now on the media are treated as two other cell types).

To model resistance of the cells and internal medium to compression, we consider also an area constraint term besides the surface energy. This second term is taken to be proportional to the square of the deviation of each cell area from its target area, $A_T(S)$, defined for each cell type and medium. The parameter $\lambda$ plays the role of a Lagrange multiplier for this constraint and regulates cell compressibility. The complete energy used in the Monte Carlo protocol is

$$H = \sum_{ij} \sum_{i'j'} E_{S_{ij}, S_{i'j'}} (1 - \delta_{S_{ij}, S_{i'j'}}) + \lambda \sum_{S} [a(S) - A_T(S)]^2 , \tag{1}$$

where $a(S)$ is the area of cell $S$, $S_{ij}$ is the spin at site $(i, j)$, and $E_{S_{ij}, S_{i'j'}}$ is the interaction energy between neighboring sites labeled by $S_{ij}$ and $S_{i'j'}$. If $S_{ij} = S_{i'j'}$ then $E_{S_{ij}, S_{i'j'}} = 0$ since in this case both sites belong to the same cell.

We implement the simulations as follows. At each time step we randomly choose a lattice site $(i,j)$ and one of its eight closest neighbors. We then propose that the site assumes the neighboring spin value $S'$ and accept with probability $P$:

$$P(S \to S') = \begin{cases} \exp(-\Delta H/T) & \text{if } \Delta H > 0\,, \\ 1 & \text{if } \Delta H \leqslant 0\,, \end{cases} \tag{2}$$

where $\Delta H$ is the variation in energy produced by the change of spin values. The unit of time, a Monte Carlo step (MCS), is taken as $L^2$ exchange attempts, where $L^2$ is the total number of sites in the lattice. To simulate slow liquid influx, the target area of the internal medium increases by one unit per Monte Carlo step, approximating a thermodynamic quasi-static process.

In this model the simulation temperature $T$ relates to active cell membrane motion. Higher $T$ implies higher membrane activity and vice-versa. $T$ simulates membrane fluctuations driven by the cytoskeleton in real cells and should not be confused with much smaller fluctuations due to thermal energy [19].

We use a square lattice with $300 \times 300$ sites and an initial circular aggregate with an internal cavity filled with (internal) medium surrounded by a monolayer of cells of the same type. The results show that in this case compression energy costs, ruled by the values of target areas, determine the essential dynamics of bursting. This happens because when individual cells deform easily their aggregates are robust, delaying bursting and swelling more. Cell size, determined by the cell target area, strongly determines how easily a cell may be deformed, whereas the number of cells in the aggregate regulates the fluctuations in the cell monolayer width, which is a relevant cause of bursting. We then considered three batches of simulations to investigate the effect of varying both cell numbers and target areas. Simulation batches A and B set cell target area $A_T = 225$ sites with $N = 12$ and 24 cells, respectively, in the monolayer, while simulation batch C considers cell target area $A_T = 117$ sites and $N = 24$ cells in the monolayer. In each batch we monitored runs with three different temperatures and five values of cell–cell adhesion energy $E_{cc}$. For each set of parameters we performed ten different runs with different random numbers sequences. Qualitatively, the behaviors of all batches are the same, and equal target areas caused aggregates in batches A and B to burst when the cells in the monolayer had stretched equal amounts. Finally, we note that we can set $\lambda = 1$ since only ratios such as $E_{cc}/\lambda$ and $T/E_{cc}$ matter. Also, the values of interaction energies are such that deviations from target area imply comparatively high energy costs and cells and internal medium behave as if filled with nearly incompressible fluids.

External medium surrounds the aggregate. Internal and external media are taken to be neutral with respect to each other, mixing perfectly ($E_{M_iM_e} = 0$). External medium has no area constraint, so its area varies freely. An area constraint on the internal medium, also with $\lambda = 1$, and a gradually increasing target area simulate the constant liquid influx to the cavity. The surface tensions ($\sigma$) on the interfaces between cells and internal and external media—$M_i$ and $M_e$—derive from the coupling energies in

Eq. (1) by

$$\sigma_{cM_i} = E_{cM_i} - \frac{E_{cc}}{2}\,,$$
$$\sigma_{cM_e} = E_{cM_e} - \frac{E_{cc}}{2}\,, \tag{3}$$

where $E_{cc}$ is the interaction energy between cells and $E_{cM}$ between cells and media [17–21]. Interaction energies between cells and media are equal with $E_{cM_e} = E_{cM_i} = 16$ (energy units/length unit) making the surface tensions between cells and both media to be the same and we will drop the subindices in what follows. In different simulation runs, the coupling energy between cells in the ring varies from $E_{cc} = 10$ to 20, so $\sigma$ varies from 6 to 11 (energy units/length unit).

Here we consider only one cell layer, of either endodermal or ectodermal cells. For multiple layers we must take into account that the presence of mesoglea might polarize cells [1], which we plan to investigate in a future study. Our present goal is to test the power of differential adhesion to explain experimental swelling and bursting of regenerating aggregates. The dynamics minimizes the interfacial energy of a ring of adherent cells constrained to envelope an incompressible internal fluid. The interaction energy between cells in the ring is lower than the energy between cells and the media and hence the lowest energy state corresponds to a compact cell aggregate without internal medium, that is, the initial pattern is metastable. The aggregate may reduce adhesion energy by expelling the internal medium, but for that an energy barrier must be surpassed and the wider the ring, the higher the energy barrier.

When the cell monolayer is thin enough, membrane fluctuations may open a hole in the cell ring and allow the internal fluid to flow out, causing a transition from the initial metastable state to the compact aggregate. As temperature is constant during the simulation, ring rupture is not caused by an increase in the fluctuation amplitude but by the thinning of the ring as the area of internal medium increases. As long as the fluctuations are not enough to break the wall, all measured quantities behave smoothly. Preliminary results of simulations in three dimensions show that after expelling some of the internal medium the cell shell heals and closes, conserving some of the internal medium, swelling again, and repeating the burst, as experimentally observed.

## 5. Simulations results

We monitored the areas of the cells and the internal medium area as the internal medium target area is increased by one unit each Monte Carlo step. We found that the internal medium area ($a_i$) grows linearly in time and we used $a_i$ as our unit of time. We also found that both cells and internal medium are always slightly smaller than their respective target areas, so a small increase in area of cells in the ring or of internal medium decreases the target area energy term. Consequently, the drive to restore areas to their target values creates an outward pressure exerted by the cells on

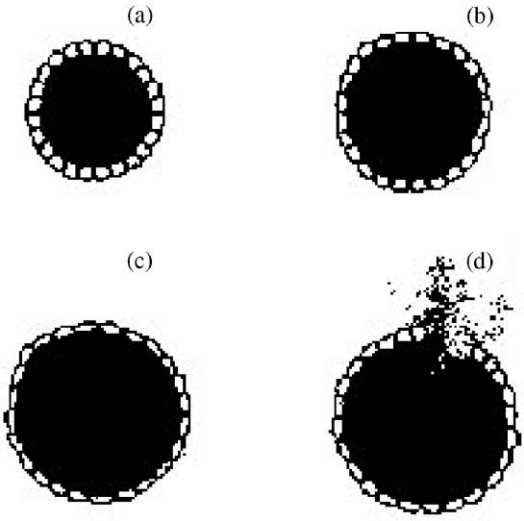


Fig. 2. Snapshots of the time evolution of a simulated aggregate with 24 cells of target area 117 sites (batch C). (a) 10 MCS, (b) 210 MCS, (c) 500 MCS, (d) 520 MCS.

their membranes and by the internal medium on the cells. The result is that the enveloping cell monolayer stretches, elongating the cells and increasing the contact length between ring cells and media and thus increasing adhesion energy. On the other hand, the drive to restore the contact length to smaller values contributes with an inward pressure exerted on the internal medium. The equilibration of the inward pressure, due to the adhesion energy, and the outward pressure, due to cell and internal medium compression, determines the aggregate radius for each value of the internal medium target area. Also, it is worth noting that as $\lambda$ is relatively large, after equilibration cells are always close to their target area values ($a(S)/A_T(S) > 0.92$) so the related energy contribution is small.

Fig. 2 presents snapshots of the time evolution of one simulation for batch C ($N = 24$ cells and $A_T = 117$) for $T = 15$ and $\sigma = 8.5$. The cells elongate and the ring thins as the cavity area increases and eventually bursts, expelling the internal medium. At this point the cells start to round up again to minimize their contact length with both media (Fig. 3). As the two loose ends of the monolayer do not reconnect, aggregates may never heal after a burst in two dimensions.

Fig. 4 shows the total energy as a function of internal area $a_i$ for batch C, from the initial time up to the burst. The slope in this graph is the internal pressure, as shown below. The total energy is

$$H = H_{adh} + H_{cells} + H_{int}\,, \tag{4}$$

where $H_{adh}$, $H_{cells}$, and $H_{int}$ are, respectively, the energy contributions from the adhesion, cell area, and internal medium area terms. Differentiating Eq. (4) with respect

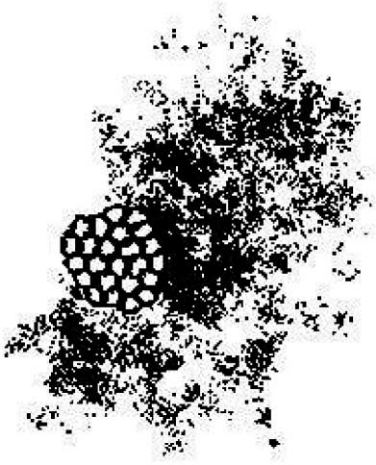

Fig. 3. Final state of an aggregate with 24 cells of target area 117 sites (batch C) after 990 MCS.

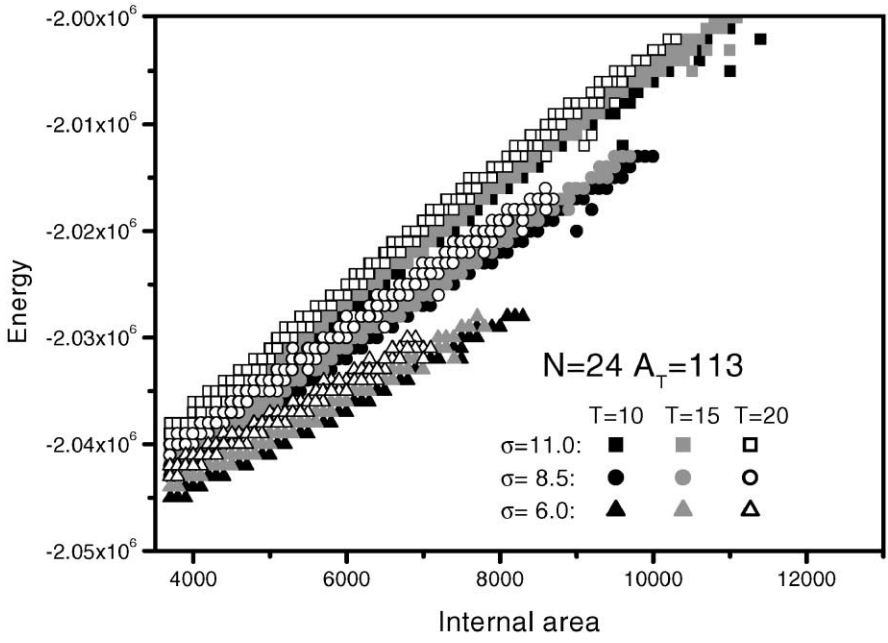


Fig. 4. Plot of the total energy as a function of the area of the internal medium for batch C (24 cells of target area 117 sites) and surface tensions 6, 8.5, and 11. The inset lists corresponding temperatures.

to the total area ($A_{tot}$) yields the pressure. Since $A_{tot} = \sum_S a(S) + a_i$ and $\sum_S a(S)$ is approximately constant, we may write

$$P_{tot} = \frac{\partial H}{\partial A_{tot}} = \frac{\partial H}{\partial a_i} . \tag{5}$$

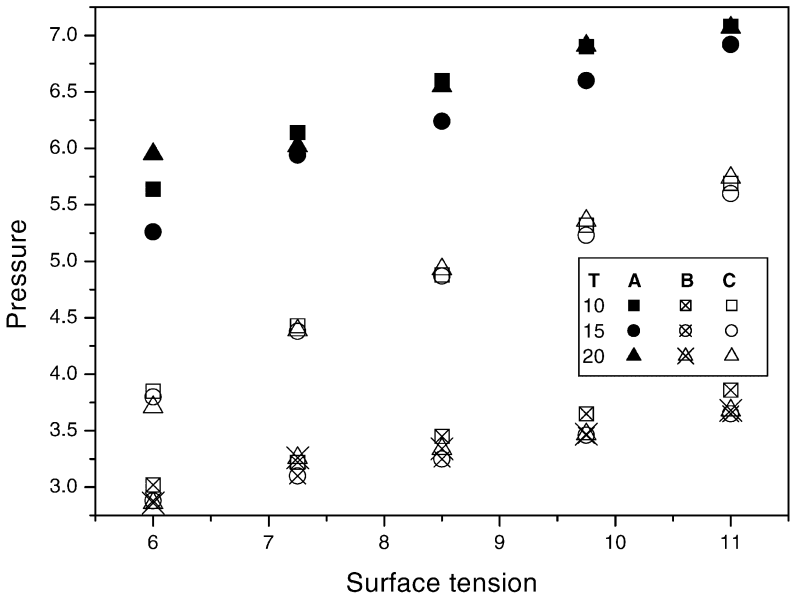


Fig. 5. Internal pressure of the aggregates for surface tensions 6, 7.25, 8.5, 9.75, and 11. The number of cells and cell target area for batches A, B, and C are, respectively, 12 cells and 225 sites, 24 cells and 225 sites and finally 24 cells and 117 sites.

In Fig. 4 we see no signaling that a burst will occur before it does, in accordance with experiments in which the aggregate swelling is quasi-static until the moment of bursting. In fact the swelling is so slow that no change is perceptible over time intervals of less than 1 h. We show data for different temperatures and surface tensions between cells and media. Following our data we note that, for the chosen parameters values, temperature effects are less important than values of surface tension, since the curves cluster into three sets determined by their surface tensions. The plots are straight lines, showing constant pressure during aggregate swelling. All our simulations show qualitatively similar behavior.

Fig. 5 plots the pressure as a function of the surface tension of the aggregates, for different temperatures and the three batches. The simulations with more cells show smaller relative fluctuations in pressure, as expected. Pressure in the three batches differ, but all increase with surface tension. Batches A and C, with different numbers of cells (12 and 24) and different target areas (225 and 117), have roughly the same ring area for the same internal medium area. However, pressure is clearly smaller for batch C aggregates where the target area is smaller. The reason is that pressure reflects the energy per total area stored in adhesion and target area deviations. To understand this effect, consider the case of two circular rings with the same internal and external radii, $R_i$ and $R_e$, respectively, and the same areas $a_R = \pi(R_e^2 - R_i^2)$, one with $n$ equal cells of target area $a_T$, and the other with $2n$ equal cells of target area $a_T/2$.

Considering the energy defined in Eq. (1), the energies of the rings are

$$E(n) = E_{cM_e} 2\pi R_e + E_{cM_i} 2\pi R_i + nE_{cc}(R_e - R_i) + n\lambda(a_R/n - a_T)^2,$$

$$E(2n) = E_{cM_e} 2\pi R_e + E_{cM_i} 2\pi R_i + 2nE_{cc}(R_e - R_i) + 2n\lambda(a_R/(2n) - a_T/2)^2, \qquad (6)$$

so $E(n) - E(2n) = n\lambda(a_R/n - a_T)^2/2 - nE_{cc}(R_e - R_i)$. For large internal areas, the ring stretches and $R_e - R_i$ is small. Hence, for large $\lambda$, energy in the $2n$ cells aggregate with half target area is smaller, implying smaller pressure, since total area is the same for both systems.

Turning our attention to batches A and B, we compare aggregates with the same target area (225) cells, but different numbers of cells (12 and 24). In this case, pressure is smaller for the aggregates with more cells because they stretch less, decreasing the target area energy. Also, a larger fraction of the cells perimeters are shared between two cells rather than cell and medium, reducing adhesion energy. Consequently, the stored energy is smaller for ring aggregates with more cells.

Thus, these simulations show that both smaller target areas and larger numbers of cells reduce the pressure in the aggregates. This result holds when interface minimization determines cell shape and effects of the cytoskeleton, rigid membranes or other specialized mechanisms are not considered.

Eq. (6) shows that the same total stretching of the aggregate costs less energy for monolayers with more cells with smaller target areas, that is, a smaller target area implies more compressible cells. For an isolated cell in external medium, the optimal geometry is a round cell that maximizes its area for a given perimeter. Deviations from a circle reduce areas for the same perimeter and, for the cells in the stretched ring, increase deviations from the target area. When the internal area grows, the cell ring stretches more and the cells become thinner, with both target area and adhesion energy terms increasing. In this case, more deformable (smaller) cells which can elongate more and form wider cell–cell interfaces, are more robust to membrane fluctuations capable of opening a hole in the monolayer. Consequently, for aggregates with the same ring area (i.e., batches A and C) bursting occurs later when the ring contains more cells with smaller target areas.

In Fig. 6 we plot time (internal area) at burst as a function of surface tension. Clearly, batch C simulations burst after batch A for the same surface tension and temperature. Batch B simulations burst still later because the ring area is larger and it must swell more before stretching to a critical value. In Figs. 7 and 8 we plot the ring width and average area of the cells at the moment of bursting as a function of the surface tension for the three batches. The ring widths at burst are similar for batches A and B but are larger for batch C simulations, indicating that the cells deformed less, deviating less from the target area, consistent with earlier bursting. In other words, rounder less deformed cells form shorter cell–cell interfaces and hence are more vulnerable to bursting. Also, average cell area and ring width at burst are the same for batches A and B, which have equal target areas.

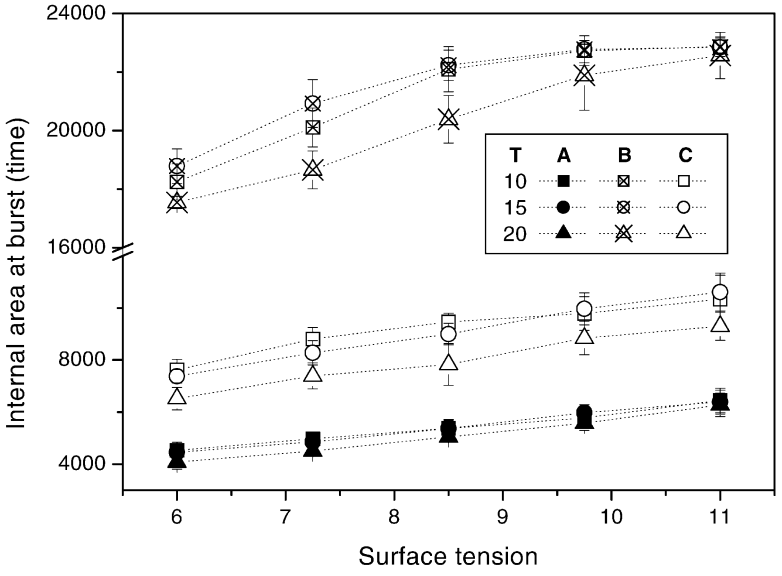


Fig. 6. Area of the internal cavity at burst for surface tensions 6, 7.25, 8.5, 9.75, and 11. The number of cells and cell target area for batches A, B, and C are, respectively, 12 cells and 225 sites, 24 cells and 225 sites and finally 24 cells and 117 sites.

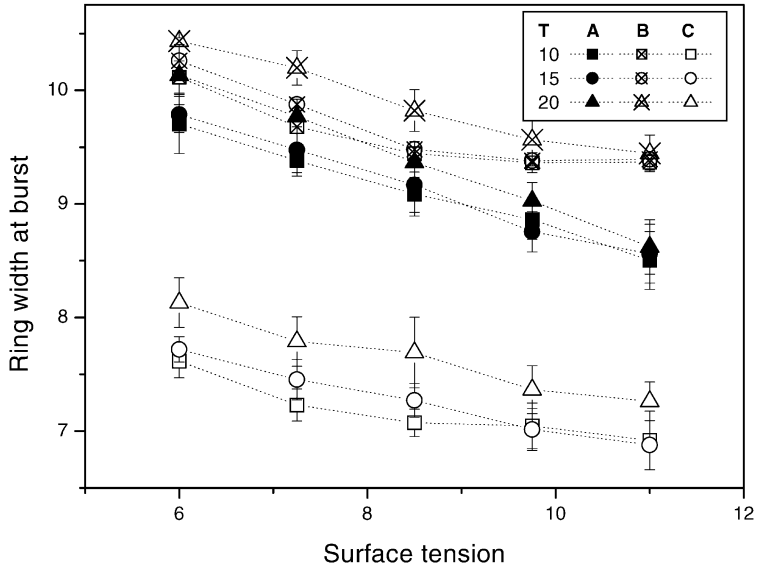


Fig. 7. Plot of the average width of the monolayer at burst for surface tensions 6, 7.25, 8.5, 9.75, and 11. The number of cells and cell target area for batches A, B, and C are, respectively, 12 cells and 225 sites, 24 cells and 225 sites and finally 24 cells and 117 sites.

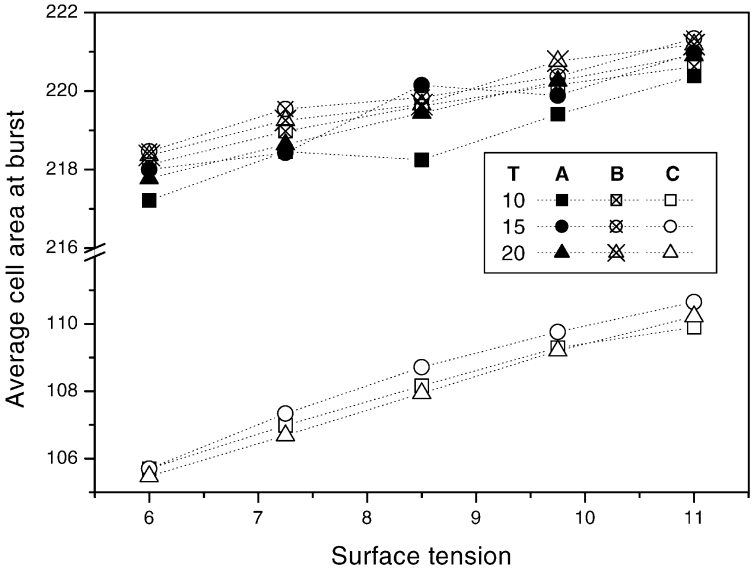


Fig. 8. Plot of the average area of the cells at burst for surface tensions 6, 7.25, 8.5, 9.75, and 11. The number of cells and cell target area for batches A, B, and C are, respectively, 12 cells and 225 sites, 24 cells and 225 sites and finally 24 cells and 117 sites.

## 6. Conclusions

Bursts in regenerating aggregates of *Hydra* cells simultaneously expel internal liquid and loose cells. We suggest that these bursts are a consequence of internal pressure caused by liquid influx that, in an intact animal, are essential to prevent internal cavity collapse.

To test this hypothesis we performed numerical simulations in two dimensions and showed that differential adhesion theory with boundary conditions that simulate liquid flow into the internal cavity reproduces the main qualitative features of the bursts: the aggregates swell, the cell monolayers thin down to a critical thickness and burst. The simulations also predict that aggregates of smaller cells have lower internal pressure and burst later than same size aggregates containing fewer, larger cells. Also, larger surface tensions between cells and media generate higher internal pressure. Differential adhesion mechanisms and liquid influx suffice to explain bursts in cell aggregates.

Our experiments used small aggregates which burst before they elongate, a necessary step for complete *Hydra* regeneration. Larger aggregates take longer to burst. In these cases, muscular contractions can also occur and influence the bursts. We are currently investigating the dependence of burst dynamics on initial aggregate size.

## Acknowledgements

Support for this work includes the scientific exchange collaboration program CNPq-NSF (INT-98-02417). We acknowledge partial financial support from Brazilian agencies FAPERGS, CNPq, and FINEP. DE-FG0299ER 45785 and from the U.S., NSF CTS-9601691.

## References

[1] S.F. Gilbert, Developmental Biology, Sinauer, Sunderland, 1991.
[2] A. Gierer, S. Berking, H. Bode, C.N. David, K. Flick, G. Hansmann, H. Schaller, E. Trenkner, Regeneration of hydra from reaggregated cells, Nat. New Biol. 239 (1972) 98–101.
[3] P.A. Townes, J. Holtfreter, Directed movements and selective adhesion of embryonic of amphibian cells, J. Exp. Zool. 128 (1955) 53–120.
[4] M.S. Steinberg, Reconstruction of tissues by dissociated cells, Science 141 (1963) 401–408.
[5] G. Forgacs, R.A. Foty, Y. Shafrir, M.S. Steinberg, Viscoelastic properties of living embryonic tissues: a quantitative study, Biophysics J. 74 (1998) 2227–2234.
[6] P.B. Armstrong, Cell sorting out: the self-assembly of tissues in vitro, CRC Crit. Rev. Biochem. Mol. Biol. 24 (1989) 119–149.
[7] N. Kataoka, K. Saito, Y. Sawada, NMR microimaging of the cell sorting process, Phys. Rev. Lett. 82 (1999) 1075–1078.
[8] G.S. Davis, H.M. Philips, M.S. Steinberg, Germlayer surface tension and "tissue affinities' in *Rana pipiens* gastrulae: quantitative measurements, Deve. Biol. 192 (1997) 630–644.
[9] J.C.M. Mombach, Simulation of embryonic cell self-organization: a study of aggregates with different concentrations of cell types, Phys. Rev. E 59 (1999) R3827–R3830.
[10] J.C.M. Mombach, Universality of the threshold in the dynamics of biological cell sorting, Physica A 276 (2000) 391–400.
[11] J.A. Glazier, unpublished experimental data, 2000.
[12] I. Smid, P. Tardent, The influences of ecto- and endoderm in determining the axial polarity of *Hydra attenuata* Pall, Wilhelm Roux's Archives 191 (1982) 64–67.
[13] K.M. Flick, H.R. Bode, Dissociated tissues into cells and the development of hydra from aggregated cells, in: H.M. Lenhof (Ed.), "Hydra: Research Methods", Plenum, New York, 1983, pp. 251–260.
[14] D. Benos, R.G. Kirk, W.P. Barba, M.M. Goldner, Hyposmotic fluid formation in Hydra, Tissue and Cell 9 (1977) 11–22.
[15] M.P. Sarras Jr., X. Zhang, J.K. Huff, M.A. Accavitti, P.L. St. John, D.R. Abrahamson, Extracellular matrix (mesoglea) of Hydra Vulgaris, Deve. Biol. 157 (1993) 383–398.
[16] S.E. Fraser, C.R. Green, H.R. Bode, N.B. Gilula, Selective disruption of gap junctional communication interferes in a patterning process in hydra, Science 237 (1987) 49–55.
[17] F. Graner, J.A. Glazier, Simulation of biological cell sorting using a two-dimensional extended Potts model, Phys. Rev. Lett. 69 (1992) 2013–2016.
[18] J.A. Glazier, F. Graner, Simulation of the differential adhesion driven rearrangement of biological cells, Phys. Rev. E 47 (1993) 2128–2154.
[19] J.C.M. Mombach, J.A. Glazier, R.C. Raphael, M. Zajac, A quantitative comparison between differential adhesion models and cell sorting in the presence and absence of fluctuations, Phys. Rev. Lett. 75 (1995) 2244–2247.
[20] J.C.M. Mombach, J.A. Glazier, Single cell motion in aggregates of embryonic cells, Phys. Rev. Lett. 76 (1996) 3032–3035.
[21] F. Graner, Can surface adhesion drive cell-rearrangement? Part I: biological cell-sorting, J. Theor. Biol. 164 (1993) 455–476.